This article has been accepted for publication in IEEE/OSA Journal of Lightwave Technology. This is the author's version which has not been fully edited and content may change prior to final publication. Citation information: DOI 10.1109/JLT.2024.3406521

Detector-On-Demand Architecture for Flexible Homodyne Transmission in Optical Networks

Bernhard Schrenk, *Member, IEEE*, and Fotini Karinou, *Senior Member, IEEE*

***Abstract*—The dynamicity and heterogeneity in traffic demands necessitates an adaptation of optical transceivers to the actual network needs. While software-defined mechanisms can contribute to this challenge, hardware-oriented schemes have been hardly addressed to date. Towards this direction, we propose a multi-purpose transceiver architecture that is able to adapt its physical-layer function with respect to coherent homodyne detection and signal transmission thanks to its segmented layout that features dual-function opto-electronic elements. By synthesizing various transceiver configurations, we will experimentally show the flexible use of polarization and spectrum through switching between half- and full-duplex modes in polarization-independent or polarization-multiplexed signal transmission at up to 91 Gb/s/sub-λ data rates, while optionally supporting the ultra-dense packing of data channels and simultaneous mixed signal transmission on a single wavelength.**

***Index Terms*—Optical communication terminals, Reconfigurable devices, Optical signal detection, Optical modulation**

I. INTRODUCTION

METRO networks are expected to support Tb/s capacities while supporting flexibility with respect to highly dynamic traffic demands through a reconfigurable network architecture [1]. In such a setting, an adaptation to the actual network load and channel loss can be accomplished through exploiting freedom in the spectral allocation and modulation [2-7] or the resource partitioning with respect to additional multiplexing dimensions such as space and polarization [8]. In either of these cases, a wide range of requests can be accommodated through the involved optical transponders, ideally without the need to alter or over-provision their physical-layer hardware. Given the dynamicity that resides in optical metro networks, flexible optical transceiver engines are therefore paramount and of great advantage.

A possible solution to address this challenge has been found in software-defined transceivers. These enable a swift and – from a physical-layer perspective – zero-touch reconfiguration of transceiver parameters to adapt to the actual link requirements. Examples can be found in (sliceable) bit-rate variable transceivers [3, 4], which allow the creation of multiple co-existing yet independent virtual transceivers that share a common physical broadband transceiver hardware. In addition, a physical-layer agnostic reconfiguration of the signal processing stack can be incorporated to optimize the use of available resources [9-11]. Even though such software-defined transceivers are an elegant solution to tune modulation and bandwidth parameters without impacting the physical-layer implementation, the procedures adopted for the purpose of reconfiguration provide limits on the extent at which a physical-layer adaptation is supported.

Manuscript received March 23, 2024. This work was supported in part by the European Research Council (ERC) under the European Union's Horizon 2020 research and innovation programme (grant agreement No 804769).

B. Schrenk is with the AIT Austrian Institute of Technology, Center for Digital Safety & Security, Giefinggasse 4, 1210 Vienna, Austria (phone: +43 50550-4131; fax: -4150; e-mail: bernhard.schrenk@ait.ac.at).

F. Karinou is with Microsoft Research Ltd, Cambridge Science Park, CB4 0GW Cambridgeshire, United Kingdom (e-mail: fotini.karinou@microsoft.com).

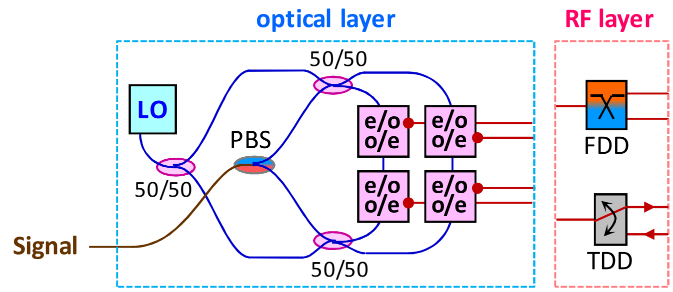

Fig. 1. Physical-layer reconfigurable transceiver architecture based on a segmented configuration of multi-purpose electro-optic pixels.

Towards this direction, we expand our initial investigation of a physical-layer reconfigurable transceiver (TRX) architecture [12] based on a segmented configuration of multi-purpose electro-absorption modulator (EAM) elements. We will investigate its performance for low-cost, high-capacity coherent OFDM transmission in various metro and access scenarios by originating from a single EAM element that is gradually advanced to a multi-purpose architecture that enables (*i*) a flexible assignment of polarization and spectrum, (*ii*) half- and full-duplex operation modes, (*iii*) support for ultra-dense wavelength division multiplexed (WDM) transmission through access to the sub-WDM dimension by means of balanced detection, and (*iv*) the simultaneous reception of mixed (i.e., digital and analogue) signals. The use of a reconfigurable element such as an EAM as detector segment is attractive since EAMs are multi-purpose elements, are featuring a high electro-optic bandwidth, are highly efficient with respect to modulation and can be implemented on a very compact and pixel-like footprint.

The manuscript is organized as follows. Section II introduces the proposed detector-on-demand architecture. Section III addresses the corresponding experimental evaluation procedures. Section IV investigates half-duplex

This article has been accepted for publication in IEEE/OSA Journal of Lightwave Technology. This is the author's version which has not been fully edited and content may change prior to final publication. Citation information: DOI 10.1109/JLT.2024.3406521

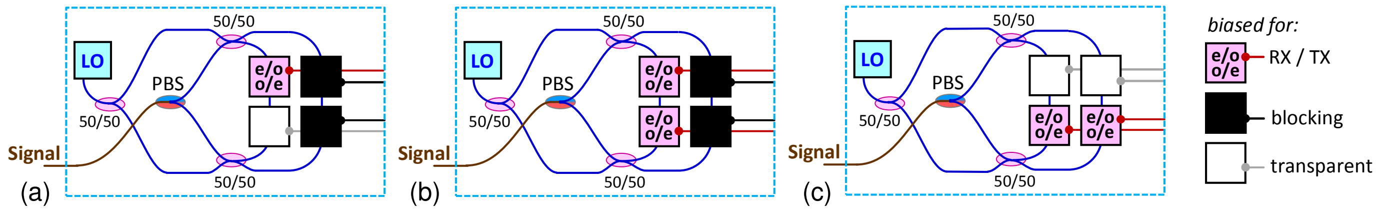

Fig. 2. Detection modes, including (a) polarisation-independent, (b) polarisation-multiplexed, (c) balanced coherent detection.

TABLE I
DETECTOR-ON-DEMAND CONFIGURATIONS.

Configuration	TRX	BW [GHz]	λ	TX pol.
❶ Half-duplex	DET-1	15 DS	λ_T	TE
❷ Full-duplex bidirectional	DET-1	6 DS, 6 US	λ_T	TE
❸ Pol independent	DET-1	15 DS	λ_T	TE scramb.
❹ Pol multiplexed	DET-2	15 DS	λ_T	TE + TM
❺ Balanced det.	DET-3	15 DS	λ_T	TE
❻ UDWDM	DET-3	15 DS	λ_T, $\lambda_{a1/2}$	TE
❼ Mixed signal	DET-1	10 OOK, 1 OFDM	λ_T	TE

transmission and reception with the multi-functional TRX. Section V discusses how polarization-independent operation can be accomplished. Section VI then introduces full-duplex transmission over the same TRX. The case of polarization-multiplexed reception is reported in Section VII, while Section VIII sheds light on a balanced detection mode in combination with ultra-dense WDM. Section IX investigates mixed signal detection under single-wavelength baseband and radio-over-fiber transmission. Finally, Section X concludes the work.

II. COHERENT DETECTOR-ON-DEMAND

Figure 1 presents the principal TRX architecture that supports coherent detection and signal transmission. It builds on a homodyne receiver layout with access to the polarization dimension in its signal branch. The conversion elements between the optical and electrical domain are arranged in a way to (*i*) support bidirectional signal transmission through a dual-function signal converter that offers opto-electronic (o/e) photodetection and electro-optic (e/o) modulation capabilities, contributed through an EAM element, and (*ii*) to operate as a 2×2 array between the complementary ports of the polarization-diversity architecture. A bidirectional mode can be additionally supported through simple radio frequency (RF) based signal duplexing, such as provided through a paired spectrum in combination with frequency division duplexing (FDD) or through time slot allocation in conjunction with time division duplexing (TDD). This enables us to accommodate asymmetric traffic demands where bandwidth can be allocated through capacity provisioning in frequency and time. At the same time, multiple signals can be jointly transmitted over the same wavelength channel and demultiplexed in the electrical domain. For example, different services can be allocated to dedicated frequency bands, such as it will be demonstrated for wired and wireless signals in the context of wireline-wireless convergence.

While the first photonic TRX aspect concerning the dual-function EAM element has been exploited in past works, as will be discussed shortly, the specific TRX architecture allows an adaptation of the TRX to its actual application setting. Figure 2 highlights representative options towards this direction. For example, the layout in Fig. 2(a) implements a dual-polarization feed at the two ports of the same inline EAM, which is accomplished by biasing the adjacent EAM of the same detector branch at transparency, meaning that the EAM deliberately passes through the signal by setting its bias to 0V. In this way, polarization-independent coherent detection can be obtained. Figure 2(b) instead doubles the capacity through access to the polarization dimension. Such dual-polarization schemes for intensity-modulation / direct-detection links have recently moved into the focus of research where they can build on integrated polarization trackers [13, 14]. In case of the proposed detector-on-demand configuration the second EAM element is not biased at transparency anymore but now serves as an independent detector. With both EAMs now biased at high absorption, the signal pass-through between the EAMs is effectively interrupted and polarization cross-talk upon photodetection is mitigated. In this way, the two EAMs coherently detect the incident polarization-multiplexed signal in both polarizations. The third configuration in Fig. 2(c) actively employs the second detector branch that is fed by the complementary light input. In this way, a balanced EAM detector configuration can be obtained, which enables a suppression of common-mode noise and direct-detection (DD) terms, such as present in spectral-efficiency enhanced ultra-dense WDM schemes.

In the experiment that follows for validating the proposed concept, the local oscillator (LO) at the TRX will be locked to the incident data signal. This ensures that the electrical signal reception remains transparent to the actual optical signal transmission since no additional digital signal processing (DSP) functions will be required to facilitate coherent detection. To do so, we will employ injection locking, for which a detailed characterization in combination with EAM-based detectors can be found elsewhere [15]. Alternative self-coherent reception schemes, such as demonstrated in [16], are not considered in this work due to the exclusive focus on single-fiber access for the TRX.

This article has been accepted for publication in IEEE/OSA Journal of Lightwave Technology. This is the author's version which has not been fully edited and content may change prior to final publication. Citation information: DOI 10.1109/JLT.2024.3406521

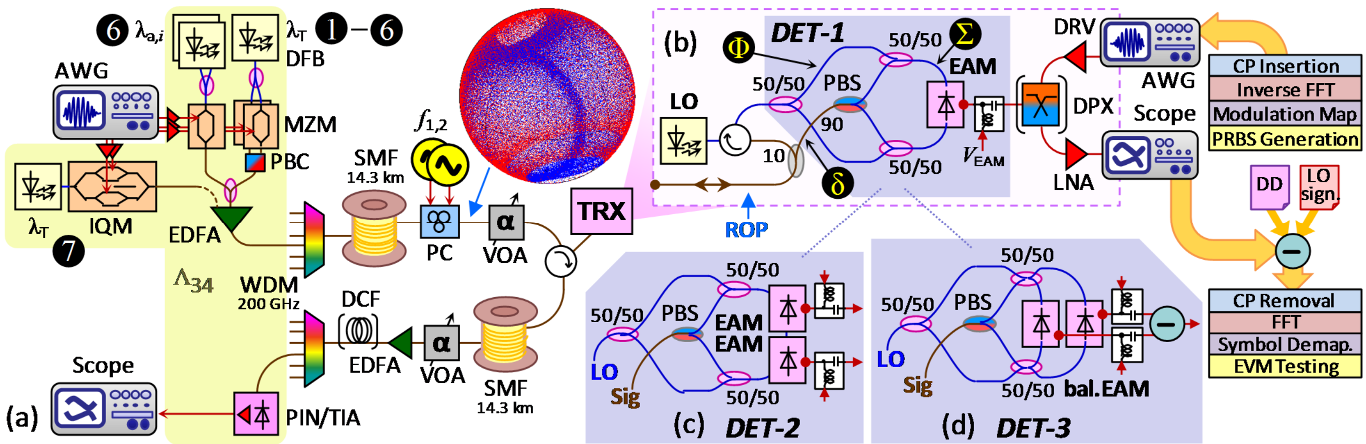

Fig. 3. (a) Experimental setup for evaluating the detector-on-demand concept and corresponding detector architectures with (b) single-ended EAM, (c) segmented EAM and (d) balanced EAMs. The inset shows the polarization-scrambled data signal.

A. Transceiver Flexibility through Multi-Purpose EAM

The EAM is a highly compact opto-electronic signal converter. Moreover, it has a large electro-optic bandwidth that can exceed 100 GHz [17]. This makes the EAM an ideal candidate for optical transmitters, either co-integrated with a laser in form of an electro-absorption modulated laser (EML), or as a (reflective) stand-alone element that is remotely seeded [18]. The EAM, however, is more than just a modulator. It can further serve the purpose of signal detection when exploiting its absorption property [19-24]. This aspect has been exploited in early research works focusing on a multi-functional EAM transceiver element, where a directional split for simultaneous transmission and direct photodetection with the EAM was accomplished by means of TDD [21] or FDD [19]. The co-integration of the EAM photodiode with a transimpedance amplifier (TIA) has been further shown [25, 26]. On top of these accomplishments, coherent homodyne detection through an EAM co-integrated with a LO in the overall form of an EML has been demonstrated [27, 28]. This coherent detection mode has been further advanced to a full-duplex coherent homodyne transceiver based on a FDD-enabled bidirectionally fed EML [29] and towards operating this transceiver bidirectionally at the same wavelength, the same frequency and the same time [30], without the need for FDD.

III. Experimental Evaluation

Figure 3(a) presents the experimental setup to evaluate the proposed multi-purpose TRX, which will be investigated for the seven scenarios listed in Table I. It builds on a distributed feedback (DFB) laser without optical isolator, which is employed as an injection-locked LO. The free-running wavelength of the DFB laser is ~1550.46 nm and it can be locked to an incident optical signal within a locking range of 5.3 GHz for an injection level of -10 dBm. This renders it stable even for a low received optical power (ROP) and a sub-optimal input state of polarization. The multi-purpose detector/modulator EAMs used for opto-electronic signal conversion had a -3dB bandwidth of 13.6 GHz and were

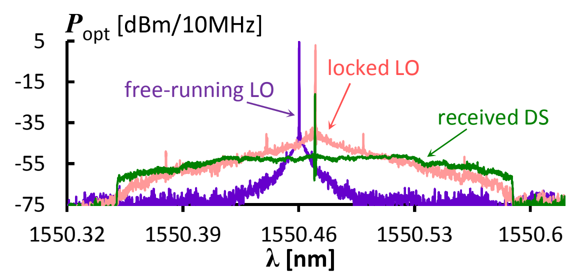

Fig. 4. Optical spectra for the 15-GHz downstream (DS) for operation in the half-duplex mode, including the LO.

biased at -1.5V. Three segmented configurations have been evaluated. The first includes a single-ended inline-EAM configuration, denoted as DET-1 in Fig. 3(b). It either detects or modulates the TE, TM polarizations at its two EAM inputs. The second is a serialized EAM layout, referred to as DET-2 in Fig. 3(c). This configuration dedicates separated electrical ports to the TE and TM polarizations. The third layout, labeled as DET-3 in Fig. 3(d), resembles a balanced EAM.

The different configurations can be realized through four EAM sections while defining the actual detector mode and thus the TRX function at the electrical domain and without change at the optical layer. Additional bidirectional full-duplex operation modes will be facilitated through slicing the RF spectrum within the bandwidth of the EAM with a RF duplexer (DPX).

It shall be noted that the injection-locked LO of the TRX provides a synchronization to the optical frequency and phase of the received signal. However, the use of fiber-pigtailed components within the experimental TRX arrangement leads to inevitable phase fluctuations between the LO and signal branches. To mitigate these undesired implementation effects, we availed of environmental stabilization and a 2-kHz linewidth laser at the head-end (λ_T) of the setup. Moreover, we employed addtitional fiber phase shifters between the signal and LO lightpaths within the TRX, taking control information from feedback on the detected RF spectrum.

Modulation-wise, we built on broadband orthogonally frequency division multiplexed (OFDM) data signals. The 128

This article has been accepted for publication in IEEE/OSA Journal of Lightwave Technology. This is the author's version which has not been fully edited and content may change prior to final publication. Citation information: DOI 10.1109/JLT.2024.3406521

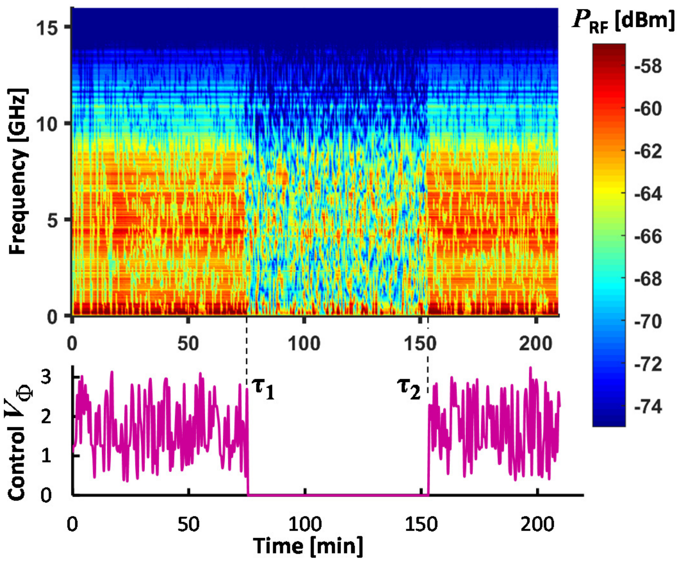

Fig. 5. Monitored RF signal detected by the EAM when stabilizing the optical phase between the LO and signal, together with the drive V_Φ of the optical phase controller.

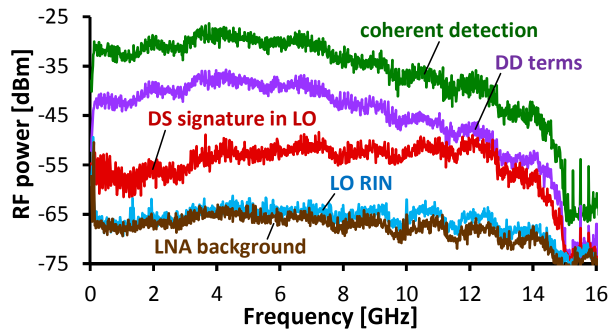

Fig. 6. Received 15-GHz DS spectra and corresponding contributions due to DD terms, its signature in the locked LO and other TRX-side noise sources.

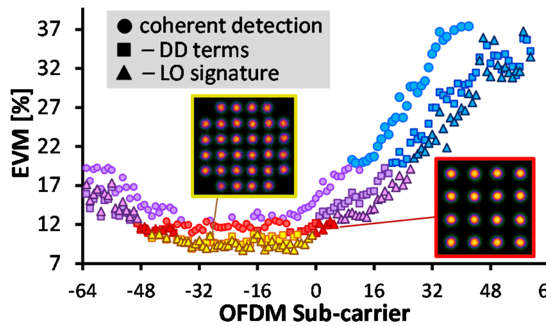

Fig. 7. EVM for back-to-back half-duplex DS reception when additionally accounting for DD terms and the LO signature.

sub-carriers of the single-polarization and polarization-multiplexed OFDM downstream (DS) from the head-end to the TRX were adaptively bit loaded. Upstream (US) signals from the TRX towards the head-end followed this OFDM setting with an individual bit loading. Two closely-spaced adjacent channels ($\lambda_{a,1/2}$) were provisioned within the ITU-channel 34 for the balanced detection scenario, together with the DS data channel λ_T at 1550.47 nm, to which the LO of the TRX unit was optically locked. Polarisation scrambling is applied to investigate the specific case of polarization-indepedent TRX operation. A pre-amplified PIN/TIA receiver was employed at the head-end to detect the US data signal transmitted by the TRX.

IV. Half-Duplex Operation

Half-duplex operation is investigated by operating the EAM at the TRX in either receive or transmit mode. Its bandwidth is fully dedicated to either DS reception or US transmission.

Figure 4 shows the optical spectra for the transmitted 15-GHz DS, together with the LO spectrum at the TRX at its free-running and locked states. The filtering effect on the DS that resides as a signature on the injection-locked LO can be well noticed.

Figure 5 exemplifies the effect of stabilizing the optical phase between the LO and signal branches of the TRX by illustrating the spectrogram of the electrically tapped signal spectrum detected by the EAM, together with the electrical drive V_Φ for the employed fiber phase shifter at point Φ in Fig. 3(b). Results are shown for a duration of 210 mins, for which the phase stabilization is interrupted after τ_0 = 76 min to demonstrate the effect of an uncontrolled optical phase. The phase fluctuation reduces the detected signal magnitude by 3.3 dB in average. The signal magnitude recovers upon re-asserting optical phase control at τ_1 = 153 min.

Figures 6 and 7 report the RF spectra and error vector magnitude (EVM) for single-wavelength and single-polarization half-duplex back-to-back (b2b) 15-GHz DS reception with the single-ended EAM detector (DET-1 in Fig. 3(b)) at a ROP of 1.8 dBm. At this high ROP level, direct-detection (DD) terms can be considered as significant. They cause a degradation in EVM and result in an average modulation efficiency of 2.41 bit/sym (●) for optimized bit loading. When additionally applying a time-synchronized feed-forward cancellation of separately recorded DD terms by means of DSP for the sole purpose of investigating the impact of these DD terms, the modulation efficiency would improve to 3.28 bit/sym (■). At the same time, residual DS components are present in the locked LO, as they are compared in Fig. 6 to the relative intensity noise (RIN) of the LO and the electrical noise of the low-noise amplifiers (LNA) preceding the EAM. We additionally cancelled this undesired LO signature by feeding forward a respective recording of these terms, taken after interrupting the DS signal at point δ in Fig. 3(b). The modulation efficiency then improves to 3.41 bit/sym (▲), which equates to an OFDM data rate of 47.1 Gb/s. Besides OFDM demodulation and the additional feed-forward cancellation functions for the DD terms and the DS signature of the LO, with the last two solely being applied for the sake of investigating penalties, no further DSP methods were required to accomplish homodyne OFDM reception, as proven through the clean sub-carrier constellations in Fig. 7. The roll-of in modulation efficiency towards higher OFDM sub-carriers derives from the limited opto-electronic bandwidth of the EAM.

This article has been accepted for publication in IEEE/OSA Journal of Lightwave Technology. This is the author's version which has not been fully edited and content may change prior to final publication. Citation information: DOI 10.1109/JLT.2024.3406521

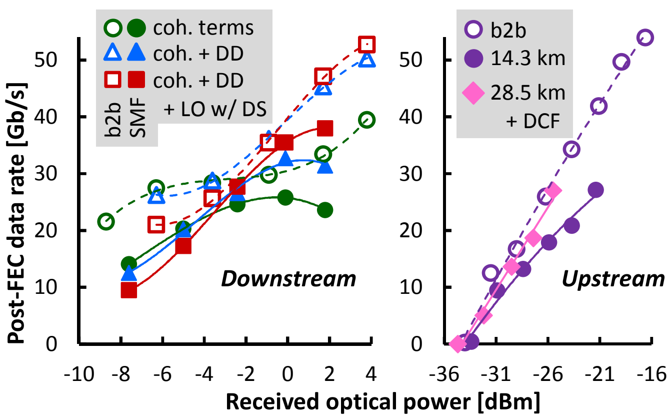

Fig. 8. Half-duplex DS and US OFDM data rate as functions of the ROP.

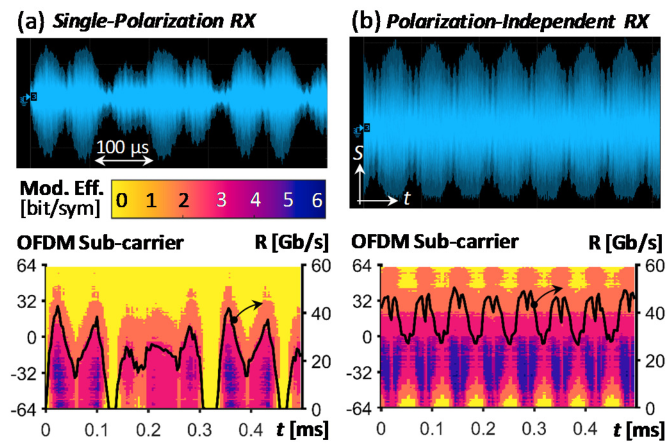

Fig. 9. Modulation efficiency and OFDM rate for (a) single-polarization and (b) polarization-independent DS reception.

Figure 8 summarizes the DS performance as a function of the ROP to the TRX. For b2b transmission, we can identify the single-ended TRX architecture as a limiting factor towards a higher ROP (○), based on the relatively wide gap to the obtained OFDM rate for the DSP-enhanced reception case insensitive to DD-terms (△). For fiber-based transmission over 14.3 km, the penalty in data rate (■,□) is attributed to chromatic dispersion in combination with the wideband OFDM transmission. Figure 8 further discusses the half-duplex 15-GHz US transmission performance when using the EAM exclusively as transmitter. Here, we obtain an OFDM data rate of 53 Gb/s for a ROP of -17 dBm at the input of the EDFA+PIN based US receiver (○). Dispersion-induced fading quickly deteriorates the US performance, leading to a ~40% penalty in peak rate for 14.3 km single-mode fiber (SMF) transmission (●). When additionally employing dispersion-compensating fiber (DCF) with a dispersion of -425 ps/nm at receiver of the head-end, we were able to transmit the US with negligible rate penalty over a length-matched span of 28.5 km (◆). This again confirms that the earlier seen US penalty derives from chromatic dispersion.

V. Polarization-Independent Operation

The polarization-independent TRX operation is reported in Fig. 9(a). For this, we drove the polarization controller (PC) included in the DS lightpath simultaneously at the two empirically chosen frequencies of $f_{1,2}$ = 15 and 6 kHz. These frequencies results in a well-scrambled polarization state for the received DS, as shown in the inset in Fig. 3(a). Figure 9 presents the received OFDM signal envelope and compares the supported modulation efficiency and resulting OFDM data rate between the single-polarization and polarization-independent operation modes.

We see the expected drop in modulation efficiency down to 0 bit/sym in case of the single-polarization TRX architecture (Fig. 9(a)), for which one EAM port has been left disconnected (Σ in Fig. 3(b)). On the other hand, the polarization-diversity TRX architecture that takes advantage of signal reception at both TE and TM inputs of the EAM prevents this drop in modulation efficiency. The resulting OFDM data rate stabilizes in a range between 26.5 and 50.4 Gb/s according to the best and worst case of input polarization. There is no DSP-based tracking required to support this mode of polarization-independent operation.

VI. Full-Duplex Operation

Full-duplex operation has been evaluated after incorporating FDD at the TRX through inclusion of the respective DPX at the electrical EAM port to share the available EAM bandwidth among dedicated DS and US frequency bands.

Figure 10 shows the optical spectrum for full-duplex 6-GHz DS and 6-GHz US transmission through FDD. The sharing of the EAM bandwidth can be clearly noticed through the distinct DS and US bands for which the DS is transmitted adjacent to the optical carrier, while the US is dedicated to the higher frequencies. The cross-over between DS and US bands occurs at 6.2 GHz from the optical carrier.

Figure 11(a) presents the corresponding RF spectra obtained by the EAM-based DS receiver and the EDFA+PIN based US receiver during full-duplex b2b DS+US transmission for a DS ROP of -0.5 dBm. We have further included the transfer function T_{DPX} of the RF duplexer that facilitates FDD at the TRX with its cross-over frequency of 6.2 GHz.

Without a present US signal, the received 6-GHz DS signal features a good EVM performance that allows a high modulation efficiency of 5.23 bit/sym (Fig. 11(b), ●). This result corresponds to a data rate of 29 Gb/s. When activating the US data, meaning that the same EAM element is used for both DS reception and US transmission at different frequency bands, a crosstalk note can be noticed towards the edge of the DS band defined by the DPX that will impacts the higher OFDM sub-carriers (Fig. 11(a)). Still, the introduced crosstalk is bearable, even though the US signal drive that is injected at the EAM is ~5 orders-of-magnitude stronger than the received DS signal. In this case of simultaneous US transmission at the upper RF band, the modulation efficiency of the DS drops slightly to 4.93 bit/sym (Fig. 11(b), ▲). An OFDM rate of 27.3

This article has been accepted for publication in IEEE/OSA Journal of Lightwave Technology. This is the author's version which has not been fully edited and content may change prior to final publication. Citation information: DOI 10.1109/JLT.2024.3406521

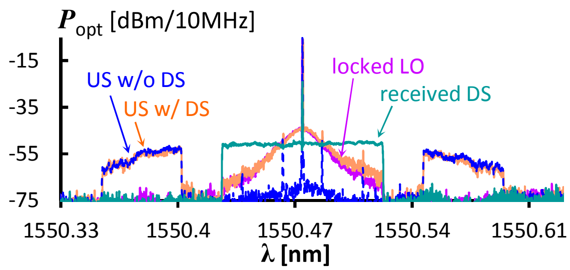

Fig. 10. Optical spectra for full-duplex 6-GHz DS/US transmission within bands defined by an FDD scheme.

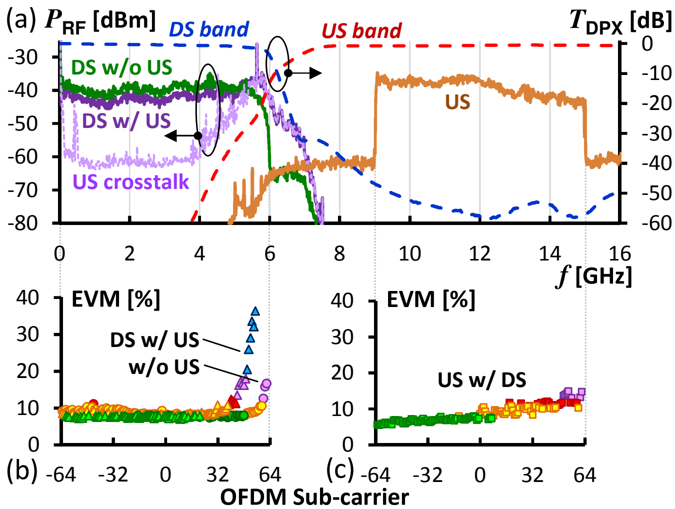

Fig. 11. (a) Received DS and US RF spectra in full-duplex mode and corresponding EVM for (b) the DS and (c) the US.

Gb/s is then supported. This proves the successful wavelength- and physical-layer hardware-sharing for DS and US data transmission. Figure 11(c) presents the EVM performance for full-duplex US transmission. The modulation efficiency for the US was 4.82 bit/sym (■) for a ROP of -17 dBm at the EDFA+PIN US receiver, equivalent to an OFDM rate of 26.7 Gb/s.

Figure 12 summarizes the OFDM rates for full-duplex DS (▲,■) and US (●,◆) transmission in the b2b case and over SMF. When compared to the half-duplex 6-GHz DS, we see a rate penalty of 9% to 35% for full-duplex transmission (▲,■) over the entire range of ROP. The reduced DS signal bandwidth of 6 GHz prevents an additional dispersion-induced penalty. The US performance is widely independent of the presence of DS data. This can be expected since the US reception is not impacted by crosstalk conditions as they incur for the DS reception. Concerning chromatic dispersion, we see similar conditions applying as for the half-duplex 15-GHz US transmission (Fig. 8). This is attributed to the spectral allocation of the US at the upper RF band of the FDD scheme.

VII. Polarization-Multiplexed EAM Detection

Polarization-multiplexed reception was investigated for the segmented EAM layout in the DET-2 architecture of Fig. 3(c). Figure 13 presents the transmitted DS spectrum, which features two 15-GHz tributaries in the TE and TM

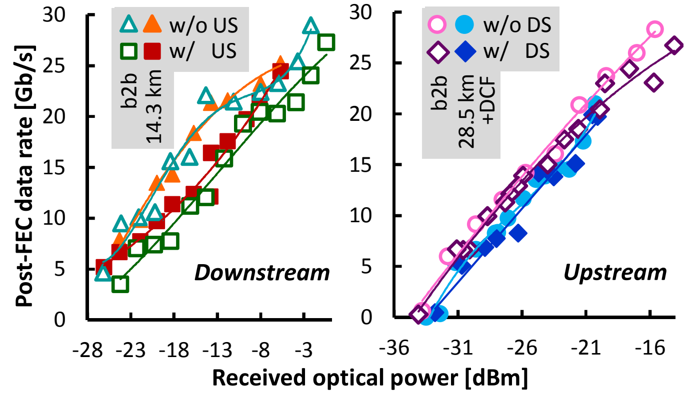

Fig. 12. Full-duplex DS and US OFDM data rate as functions of the ROP.

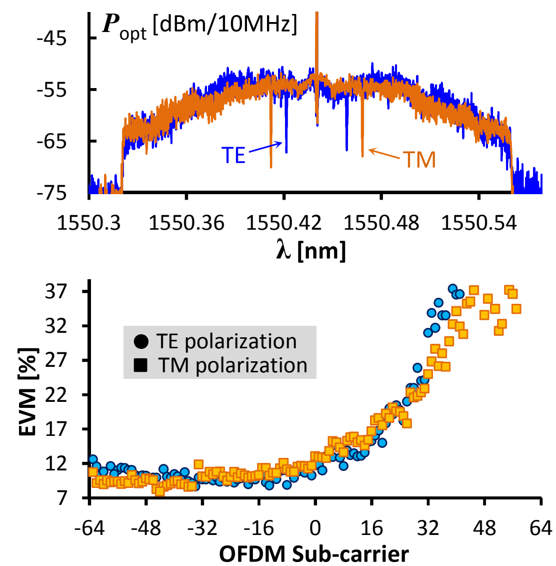

Fig. 13. Optical spectra for polarization-multiplexed DS reception and corresponding EVM performance.

polarizations. These tributaries feature a distinctive notch at one of its OFDM sub-carriers, as indicated in Fig. 13. The input polarization to the TRX was then aligned according to the visibility of these notches in either of the two detected EAM signals, resulting in an optimal separation of the TE and TM signals at the respective EAM detector. The EVM, taken for a ROP of 4 dBm, shows average modulation efficiencies of 3.41 and 3.21 for TE and TM polarizations. This permits an increased OFDM rate of 91.6 Gb/s in total.

VIII. Balanced EAM Detection

The balanced EAM detection was evaluated for the dual-branch EAM layout in the DET-3 architecture of Fig. 3(d). Figure 14(a) presents the transmitted DS spectrum with the target channel at λ_T and its two adjacent channels $\lambda_{a,1/2}$. These three simultaneously transmitted data channels create an ultra-dense WDM scheme with 34-GHz channel spacing within the ITU-T DWDM channel Λ_{34}. Figure 14(b) reports the detected RF signal spectrum for the DS channel at λ_T. We notice an improvement of ~14 dB in average for the suppression of DD

This article has been accepted for publication in IEEE/OSA Journal of Lightwave Technology. This is the author's version which has not been fully edited and content may change prior to final publication. Citation information: DOI 10.1109/JLT.2024.3406521

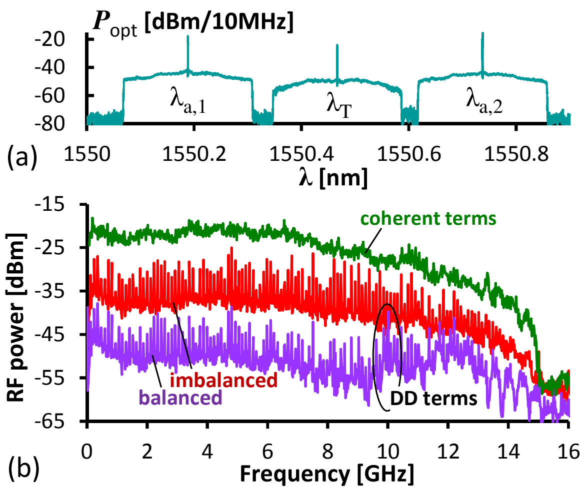

Fig. 14. (a) Optical spectrum for ultra-dense WDM within ITU-T channel Λ_{34}, and (b) RF spectra for single-ended and balanced EAM detection of the DS channel at λ_T.

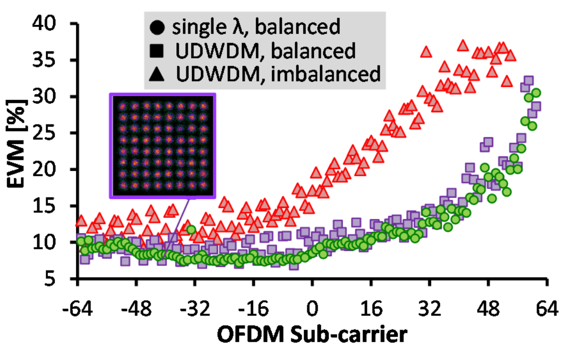

Fig. 15. EVM performance under balanced EAM detection.

terms and adjacent channel noise due to the balanced EAM operation.

The EVM performance under balanced operation is presented in Fig. 15. The penalty in terms of modulation efficiency arising from the adjacent channels $\lambda_{a,1/2}$ under imbalanced EAM operation (▲) can be entirely recovered through the balanced EAM configuration (■), enabling a single-polarization OFDM rate of 58.8 Gb/s for a ROP of 4 dBm. This rate under balanced EAM operation is very similar to the OFDM rate for single-channel transmission at λ_T (●), which was 62.4 Gb/s. Moreover, the balanced EAM detector configuration does not require digital compensation concerning the DD terms or the DS signature in the LO to accomplish these high OFDM rates, as it was required for the single-ended EAM detector employed in Section IV.

IX. Mixed Signal Detection

Finally, the coherent detection of mixed signals has been investigated in a representative scenario that combines digitized and analogue radio-over-fiber transmission for joint antenna remoting of macro- and small-cells. In this setting, the TRX performs the simultaneous detection of heterogeneous signals that are present on the same wavelength, as will be proven for the reception of on-off keyed (OOK) and OFDM signals.

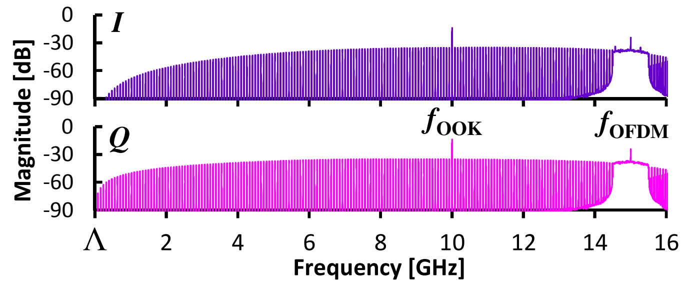

Fig. 16. AWG drive for independent sideband modulation resulting in mixed OOK and OFDM signal transmission.

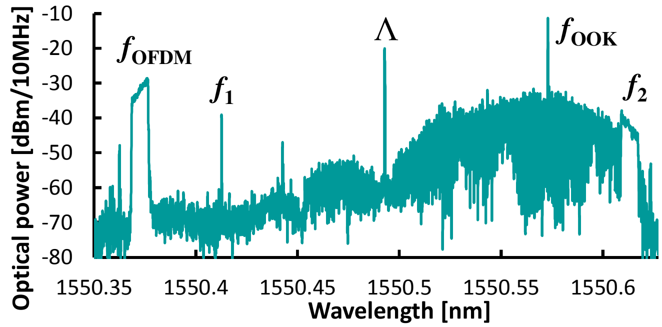

Fig. 17. Optical spectrum of the independently modulated sidebands of Λ, hosting OOK and OFDM signals.

We employed independent sideband modulation [31] to facilitate the joint transmission of a 10 Gb/s OOK data signal and an OFDM signal with 128 sub-carriers loaded by 16-QAM data over a bandwidth of 1 GHz. Moreover, the OFDM signal is intended to be up-converted to a FR2 band frequency of 25 GHz. To accomplish all these, the OOK signal is first modulated on an auxiliary carrier of f_{OOK} = 10 GHz relative to the optical carrier Λ = 1550.47 nm, while the OFDM signal is situated at a relative carrier frequency of f_{OFDM} = 15 GHz. Independent sideband modulation through an optical inphase/quadrature modulator (IQM), as introduced in the setup in Fig. 3(a), then ensures that these two signals are modulated at the upper and lower sideband of the carrier Λ, respectively.

The corresponding drive signals for the IQM are composed by the pseudo-random OOK and OFDM signals and their spectra are presented in Fig. 16. Even though the OOK and OFDM signal spectra overlap in the electrical domain, there is a good sideband suppression for each of them, as confirmed through the optical output spectrum of the IQM reported in Fig. 17. Here, we see a suppression of 28 and 9.2 dB in the second sideband for the OOK signal (f_{OOK}, f_1) and for the OFDM signal (f_{OFDM}, f_2), respectively. Moreover, the optical carrier Λ is suppressed in addition, enhancing the carrier component f_{OOK} by 8.5 dB with respect to Λ and thus making it the dominant spectral feature for the TRX to lock on. With this, the OFDM is up-converted to its target RF carrier frequency of $f_{OOK} + f_{OFDM}$ = 25 GHz. The spectral tilt in the OFDM signal is explained by the finite bandwidth of the utilized electrical amplifiers and IQM.

This article has been accepted for publication in IEEE/OSA Journal of Lightwave Technology. This is the author's version which has not been fully edited and content may change prior to final publication. Citation information: DOI 10.1109/JLT.2024.3406521

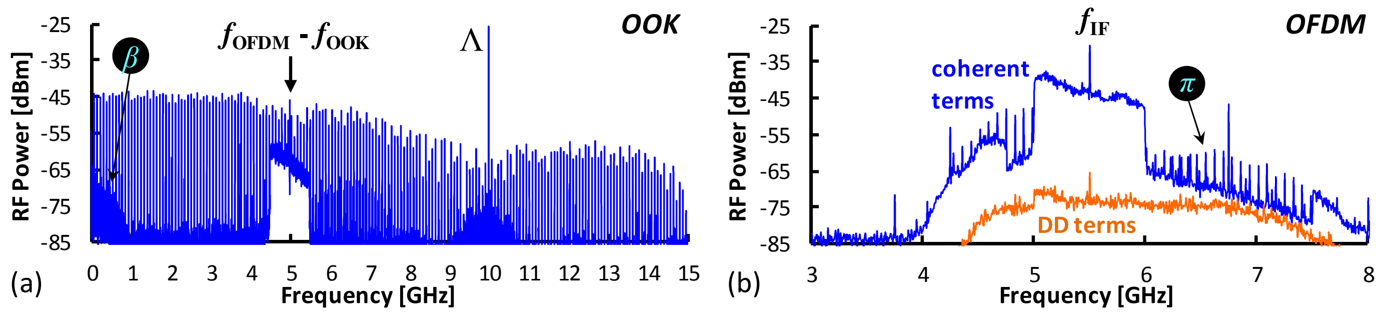

Fig. 18. Received RF signal spectra for (a) the baseband OOK signal, and (b) the down-converted K-band OFDM signal.

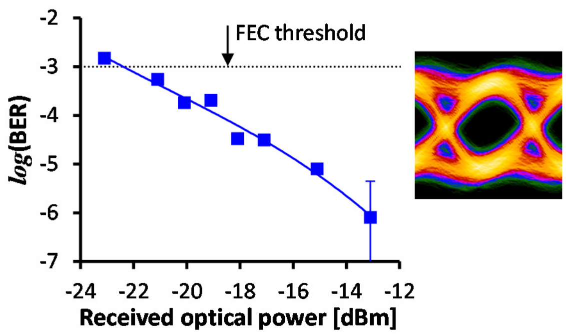

Fig. 19. BER performance for 10 Gb/s OOK transmission.

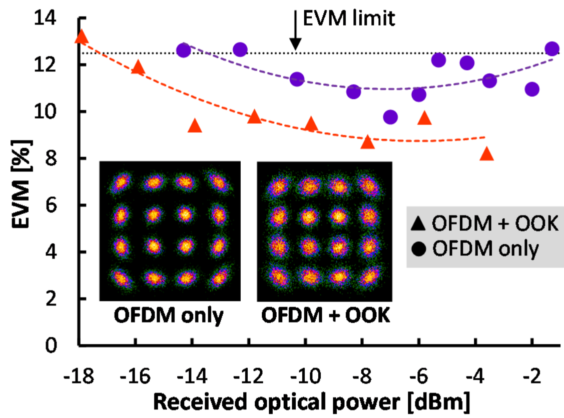

Fig. 20. EVM performance for 1-GHz OFDM transmission.

At the TRX, which would be situated at a remote radio head (RRH) site, we employ a receiver architecture according to the DET-1 layout of Fig. 3(b). However, the EAM is replaced by a 40G-rated variant with an enhanced 3-dB bandwidth in support for the detection at the K-band. The LO of the TRX now locks on the spectral feature introduced through f_{OOK}. A DPX with a cross-over frequency of 19.1 GHz then acts as frequency band demultiplexer by separating the detected digital OOK signal, which now finds itself at the baseband, from the analogue OFDM signal. After signal amplification, the OOK signal is directly evaluated in terms of bit error ratio (BER) measurement, while the OFDM signal is down-converted to an intermediate frequency (IF) of 5.5 GHz, at which it is digitized for the purpose of EVM estimation to evaluate the performance for the joint coherent detection of mixed signals on the same optical carrier.

The received RF signal spectra for the baseband OOK and the down-converted K-band OFDM signals are reported in Fig. 18 for back-to-back transmission. For the OOK signal, we see the suppressed optical carrier Λ, the beat note of the OFDM signal at $f_{OFDM} - f_{OOK}$ and the beat interference of the OFDM sub-carriers (β) as crosstalk terms. However, these terms can be either filtered or fall well below the signal magnitude of the OOK data. For the down-converted OFDM signal, its DD terms fall 34.9 dB below the coherent detection terms for a ROP of -7 dBm. Due to the co-existence of the OOK signal, further spectral harmonics (π) introduced by the pseudo-random OOK data can be noticed above the electrical noise floor of the received OFDM signal.

The reception performance of the OOK signal is presented in Fig. 19. We accomplish a reception sensitivity of -22.4 dBm at the enhanced forward error correction (FEC) threshold of 10^{-3}. This moderate sensitivity is explained by the missing electrical TIA back-end of the EAM photodiode.

The EVM performance for OFDM transmission in the K-band is presented in Fig. 20. For the joint OOK+OFDM signal detection (●), we obtain an EVM performance below the 12.5% antenna limit for 16-QAM transmission for a ROP ranging from -0.4 to -12.8 dBm. When deactivating the OOK data, the EVM for exclusive OFDM transmission (▲) improves by 2.2% and the compatible input power range expands by 3.8 dB towards lower ROP. We therefore consider this acceptable penalty for mixed signal detection accomplished by a single TRX to stand in good trade-off with a reduced complexity at the RRH site.

X. Conclusion

A hardware-oriented approach towards flexible optical transceiver technology has been investigated. By building on dual-function EAM technology to synthesize multi-purpose opto-electronic modulator/detector configurations for variety of coherent reception and transmission functions, we have experimentally demonstrated the support of a segmented TRX architecture for supporting (*i*) half- and full-duplex transmission modes through sharing of electrical spectral resources for the purpose of bidirectional transmission, (*ii*) a flexible way of how polarization is used in polarization-independent and -multiplexed detection schemes, (*iii*) the migration to the paradigm of spectrally ultra-dense signal transmission, and (*iv*) the simultaneous transmission of mixed digital and analogue signals over a single wavelength. The photonic integration of a phase-stable transceiver circuit with

This article has been accepted for publication in IEEE/OSA Journal of Lightwave Technology. This is the author's version which has not been fully edited and content may change prior to final publication. Citation information: DOI 10.1109/JLT.2024.3406521

a functionally complete 2×2 array of EAM elements is left for future work.

References

[1] L.S. de Sousa, and A.C. Drummond, "Metropolitan optical networks: A survey on single-layer architectures" *Opt. Switching and Netw.*, vol. 47, art. no. 100719, Feb. 2023.

[2] W. Shieh, "OFDM for Flexible High-Speed Optical Networks," *J. Lightwave Technol.*, vol. 29, no. 10, pp. 1560-1577, May 2011.

[3] Y. Ou *et al.*, "Demonstration of Virtualize-able and Software Defined Optical Transceiver," *J. Lightwave Technol.*, vol. 34, no. 8, pp. 1916-1924, Apr. 2016.

[4] L. Nadal, M. Svaluto Moreolo, J. M. Fabrega, and F. J. Vílchez, "SDN-Enabled Multi-Band S-BVT Within Disaggregated Optical Networks," *J. Lightwave Technol.*, vol. 40, no. 11, pp. 3479-3485, Jun. 2022.

[5] D. Welch *et al.*, "Digital Subcarrier Multiplexing: Enabling Software-Configurable Optical Networks," *J. Lightwave Technol.*, vol. 41, no. 4, pp. 1175-1191, Feb. 2023.

[6] G. Bosco, "Advanced Modulation Techniques for Flexible Optical Transceivers: The Rate/Reach Tradeoff," *J. Lightwave Technol.*, vol. 37, no. 1, pp. 36-49, Jan. 2019.

[7] R. Borkowski *et al.*, "FLCS-PON – A 100 Gbit/s Flexible Passive Optical Network: Concepts and Field Trial," *J. Lightwave Technol.*, vol. 39, no. 16, pp. 5314-5324, Aug. 2021.

[8] C. Wang, X. Xue, N. Yoshikane, F. Balasis, T. Tsuritani, and H. Guo, "Fiber-to-Application: Optical Slicing to Enhance Application Performance over a Metro Transport Network," in *Proc. Opt. Fiber Comm. Conf. (OFC)*, San Diego, United States, Mar. 2022, paper W4F.5.

[9] D. Hillerkuss, and J. Leuthold, "Software-Defined Transceivers in Dynamic Access Networks," *J. Lightwave Technol.*, vol. 34, no. 2, pp. 792-797, Jan. 2016.

[10] S. van der Heide *et al.*, "Real-time transmission of geometrically-shaped signals using a software-defined GPU-based optical receiver," *Opt. Expr.*, vol. 30, no. 15, pp. 27171-27179, Jul. 2022.

[11] P. Isautier, A. Stark, K. Mehta, R. de Salvo, and S.E. Ralph, "Autonomous Software-Defined Coherent Optical Receivers," in *Proc. Opt. Fiber Comm. Conf. (OFC)*, Anaheim, United States, Mar. 2013, paper OTh3B.4.

[12] B. Schrenk, and F. Karinou, "Detector-On-Demand for Flexible Homodyne Transmission," in *Proc. Opt. Fiber Comm. Conf. (OFC)*, San Diego, United States, Mar. 2024, paper M4F.4.

[13] X. Wu *et al.*, "Fully integrated dual-polarization silicon photonic transceiver with automated polarization control," in *Proc. Opt. Fiber Comm. Conf. (OFC)*, San Diego, USA, Mar. 2023, paper Tu2E.3.

[14] D. Che, and X. Chen, "Single-wavelength 1.2-Tb/s IM-DD transmission by polarization-multiplexing three 160-GBd PAM-8 signals," in *Proc. Europ. Conf. Opt. Comm. (ECOC),* Glasgow, UK, Oct. 2023, paper Th.C.2.8.

[15] B. Schrenk, "The Electroabsorption-Modulated Laser as Optical Transmitter and Receiver: Status and Opportunities", *IET Optoel.*, vol. 14, no. 6, pp. 374-385, Dec. 2020

[16] H. Ji *et al.*, "Photonic Integrated Self-Coherent Homodyne Receiver Without Optical Polarization Control for Polarization-Multiplexing Short-Reach Optical Interconnects," *J. Lightwave Technol.*, vol. 41, no. 3, pp. 911-918, Feb. 2023.

[17] O. Ozolins *et al.*, "100 GHz Externally Modulated Laser for Optical Interconnects," *J. Lightwave Technol.*, vol. 35, no. 6, pp. 1174-1179, Jan. 2017.

[18] L. Bogaert *et al.*, "SiPhotonics/GaAs 28-GHz Transceiver With Reflective EAM for Laser-Less mmWave-Over-Fiber," *J. Lightwave Technol.*, vol. 39, no. 3, pp. 779-786, Feb. 2021.

[19] A. Stöhr, K. Kitayama, and D. Jäger, "Full-Duplex Fibre-Optic RF Subcarrier Transmission Using a Dual-Function Modulator/Photodetector," *IEEE Trans. Microw. Theory and Tech.*, vol. 47, no. 7, pp. 1338-1341, Jul. 1999.

[20] R.B. Welstand, S.A. Pappert, C.K. Sun, J.T. Zhu, Y.Z. Liu, and P.K.L. Yu, "Dual-function electroabsorption waveguide modulator/detector for optoelectronic transceiver applications," *Phot. Technol. Lett.*, vol. 8, no. 11, pp. 1540-1542, Nov. 1996.

[21] M.P. Thakur *et al.*, "480-Mbps, Bi-Directional, Ultra-Wideband Radio-Over-Fibre Transmission Using a 1308/1564-nm Reflective Electro-Absorption Transducer and Commercially Available VCSELs," *J. Lightwave Technol.*, vol. 27, no. 3, pp. 266-272, Feb. 2009.

[22] D.S. Shin *et al.*, "Optoelectronic RF Signal Mixing Using an Electroabsorption Waveguide as an Integrated Photodetector/Mixer," *Phot. Technol. Lett.*, vol. 12, no. 2, pp. 193-195, Feb. 2000.

[23] A. Garreau *et al.*, "10 Gbit/s Drop and Continue Colorless Operation of a 1.5µm AlGaInAs Reflective Amplified Electroabsorption Modulator," in *Proc. Europ. Conf. Opt. Comm. (ECOC)*, Cannes, France, Sept. 2006, paper We.1.6.5.

[24] M. Chacinski *et al.*, "Transceiver Modules Utilizing Travelling-Wave Electro-Absorption Modulator," in *Proc. Opt. Fiber Comm. Conf. (OFC)*, San Diego, United States, Mar. 2010, paper OWN4.

[25] M. Raj *et al.*, "Design of a 50-Gb/s Hybrid Integrated Si-Photonic Optical Link in 16-nm FinFET," *J. Solid-State Circ.*, vol. 55, no. 4, pp. 1086-1095, Apr. 2020.

[26] N. Vokic, D. Milovancev, F. Karinou, and B. Schrenk, "Coherent EML+TIA Detector for DSP-Free 1 Gb/s/λ Reception Over Extended Budget," *J. Lightwave Technol.*, vol. 40, no. 14, pp. 4635-4641, Jul. 2022.

[27] B. Schrenk, "The EML as Analogue Radio-over-Fiber Transceiver – a Coherent Homodyne Approach," *J. Lightwave Technol.*, vol. 37, no. 12, pp. 2866-2872, Jun. 2019.

[28] S. Luo, Z. Li, C. Fan, X. Zhu, K. Lv, and Y. Song, "Digital mobile fronthaul based on delta-sigma modulation employing a simple self-coherent receiver," *Opt. Expr.*, vol. 30, no. 17, pp. 30684-30695, Aug. 2022.

[29] B. Schrenk, and F. Karinou, "A Coherent Homodyne TO-Can Transceiver as Simple as an EML," *J. Lightwave Technol.*, vol. 37, no. 2, pp. 555-561, Jan. 2019.

[30] B. Schrenk, and F. Karinou, "Single-Carrier, Single-λ Full-Duplex Analog Radio Feed over a Single-Port RRH Transceiver," *J. Lightwave Technol.*, vol. 41, no. 4, pp. 1114-1121, Feb. 2023.

[31] H.C. Chien, Z. Jia, J. Zhang, Z. Dong, and J. Yu, "Optical independent-sideband modulation for bandwidth-economic coherent transmission," *Opt. Expr.*, vol. 22, no. 8, pp. 9465-9470, Jan. 2014.